Published in final edited form as:
Acta Biomater. 2014 May ; 10(5): 2105–2111. doi:10.1016/j.actbio.2014.01.009.

Designing Nanogel Carriers for Antibacterial Applications

M. Carme Coll Ferrer[±,#], **Sana Dastgheyb**[§], **Noreen J. Hickok**[§], **David M. Eckmann**[#], and **Russell J. Composto**[±,*]

[±]Department of Materials Science and Engineering, University of Pennsylvania, Philadelphia, PA 19104, US

[#]Department of Anesthesiology and Critical Care, University of Pennsylvania, Philadelphia, PA 19104, US

[§]Department of Orthopaedic Surgery, Thomas Jefferson University, Philadelphia, PA 19107, US.

Abstract

Recently, we developed a novel and simple synthesis route to create nanosized (~ 5 nm) silver nanoparticles (NP) embedded in a biocompatible nanogel (NG) comprised of degradable, natural polymers, namely, dextran and lysozyme. In this study, we prepare hybrid nanogels with varying lysozyme content, evaluate their potential to reduce Ag NPs *in situ* (UV-Vis, cryo-TEM, TGA and FTIR) and determine their antibacterial properties against *Escherichia coli* and *Staphylococcus aureus*. Lysozyme enhances nucleation and stabilization of Ag NPs while limiting their growth. As lysozyme concentration increases, larger nanogels with greater loading of smaller Ag NPs are obtained. The antibacterial properties of hybrid NGs depend upon nanogel type and bacterial conditions. Hybrid nanogels with the largest Ag NPs show the lowest minimum inhibition concentration (MIC). However, the greatest bacterial killing efficiency (up to 100%) occurs within one hour if the bacteria are exposed to hybrid nanogels with smaller Ag NPs while agitating the medium. These results suggest that nanogel properties as well as antibacterial activity can be tuned by varying lysozyme content. By targeting drug delivery (e.g., ligand grafted surface), these nanogels can be used to prevent biofilm formation and control infection without the complications (i.e., over exposure) associated with classical antibiotic delivery platforms.

Keywords

dextran; lysozyme; nanogel; silver nanoparticles; antibacterial

[*]Phone +1(215)-898-4451; Fax: + 1(215)-573-2128; composto@seas.upenn.edu.
macoll@seas.upenn.edu, sana.dastgheyb@jefferson.edu, noreen.hickok@jefferson.edu, david.eckmann@seas.upenn.edu, composto@seas.upenn.edu

Introduction

Silver nanoparticles (Ag NPs) exhibit unique chemical, physical and biological properties which include high surface to volume ratio, broad optical properties, ease of synthesis as well as facile surface chemistry and functionalization. Biologically, Ag NPs show antimicrobial and anti-inflammatory properties [1-3], which are the subject of intense research aimed at using Ag NPs in disease diagnosis, treatment of infection and imaging, among many others [4, 5]. For instance, antibacterial, biocompatible coatings were developed by embedding Ag NPs (~ 5 nm) in dextran [6, 7] and Ag NPs (~ 20 nm) stabilized with egg white were used to enhance efficacy in radiotherapy for 231 tumor cells [8]. Moreover, surface enhanced Raman spectroscopy was used to detect strains of the respiratory syncytial virus using substrates composed of silver nanorods [9]. More recently, folate silver-dendrimer composite nanodevices were targeted to human epidermoid cancer cell lines, which were subsequently destroyed by microbubbles generated through uptake of laser light energy by the Ag NPs [10].

Concerns regarding the cytotoxicity of Ag NPs have motivated the development of hybrid nanogels (NG) to limit exposure of cells to Ag. Recently, we developed a novel and simple synthesis route for creating nanosized silver particles (~5 nm) inside a relatively inert and biocompatible NG (~160 nm) [7, 11]. This NG consists of a lysozyme core and a dextran shell. In particular, the shell presents multiple hydroxyls that can be used for targeting specific biological applications, ensure stability of the NG over broad ranges of pH, ionic strength and temperatures, and impart a “stealth-like” property that prevents them from recognition by the mononuclear phagocyte system [12]. By encapsulating Ag NPs in a NG, we aim to increase their efficacy while limiting their cell uptake and possible cytotoxicity. In comparison to other hybrid NG reported in the literature [13, 14], our hybrid NG are relatively green because they are prepared in aqueous solution without additional chemicals, other than the silver precursor agent, and they consist of the degradable and natural polymers, dextran and lysozyme.

In previous work, when a fixed concentration of dextran and lysozyme is used to prepare the NG (1:1, molar stoichiometry), we demonstrated that the loading of Ag in the NG can be tuned from 5 to 9 wt% by varying silver precursor concentration from 2 mM to 25 mM [11]. In this work, we first, examine the role of dextran and lysozyme in the *in situ* synthesis of Ag NPs and second, test if the resulting hybrid NGs functions as an antimicrobial agent. In contrast to previous studies, we vary the amount of dextran to lysozyme (1:1, 1:4 and 1:8, dextran:lysozyme stoichiometry) using a fixed silver precursor concentration (10 mM).

The *in situ* synthesis of Ag NPs in three distinct NGs of varying lysozyme concentration is characterized by dynamic light scattering (DLS), ultraviolet-visible spectroscopy (UV-Vis), thermogravimetric analysis (TGA) and cryo-transmission electronic microscopy (cryo-TEM). Furthermore, we explore the antibacterial properties of the hybrid NGs against *Escherichia coli* (*E. coli*) and *Staphylococcus aureus (S. aureus)*. The minimal inhibitory concentration (MIC) of the hybrid NG is evaluated using a broth microdilution method. Lastly, the effects of the hybrid NG on bacterial growth are determined as a function of time.

Materials and Methods

Synthesis of hybrid NGs

The synthesis of NGs was carried out as previously described, via a Maillard heating reaction followed by heat-gelation at 80 °C [7]. This methodology leads to core-shell type NG with a lysozyme-rich core and a dextran-rich shell [11]. Briefly, dextran (70 kDa) from *Leuconostoc* ssp. and lysozyme were dissolved (1:1, 1:4 and 1:8 molar stoichiometry) in water, the pH was adjusted to 7-8 using 0.1 N sodium hydroxide, and the solution was lyophilized. The lyophilized powder was reacted at 60 °C under 79% relative humidity in a desiccator containing saturated KBr solution for 24 h. The reacted powder was dissolved in water (5 mg/mL), the pH was adjusted to 10.7 using 0.1 N sodium hydroxide, and the solution was further reacted at 80 °C for 30 min. The resulting NG were purified by centrifugation using Amicon ultra 0.5 mL centrifugal filter devices with a 100 kDa molecular weight cut off (Millipore, Billerica, MA) and were stored in the dark at 4 °C. The final concentration of lysozyme in the NG was estimated by measuring the lysozyme concentration in the filtrate by UV-Vis. The absence of dextran in the filtrate was confirmed by Molisch assay [15]. Following purification by filtration, the final stoichiometric ratio of dextran to lysozyme is 1:0.8, 1:3.4 and 1:7.6 for NG1:1, NG1:4 and NG1:8, respectively.

The hybrid NG were prepared by mixing 2 mL of NG solution with 1 mL of 10 mM $AgNO_3$ and autoclaved for 5 min using a Sterilimatic sterilizer (Market Forge Industries Inc., Everett, MA). The free Ag NPs were separated from the NGs by dialysis in deionized water (49 mL), using a semi-permeable standard regenerated cellulose (RC) membrane (MW cut off 12-14 kDa, Spectrum Laboratories, Rancho Dominguez, CA) for 3 days.

Characterization techniques

The particle size and size distribution of the hydrated nanogels were measured by DLS using a Malvern Zetasize Nano series instrument (ZS90) equipped with a 22 mW He-Ne laser operating at a wavelength of 633 nm and analyzed with a software package (Zetasizer Nano series software Version 7.01). UV spectra of NG solution and NGs casted on glass slides were recorded in transmission on a Varian spectrophotometer (Cary 5000 UV-vis-NIR) equipped with a software package (Cary WinU Version 4.10). FTIR spectra of the drop casted solutions on cleaned silicon wafers were recorded using an attenuated total reflection accessory as a sampling system on a Perkin Elmer infrared spectrophotometer (Spectrum RX I FTIR system) at a resolution of 8 cm^{-1} averaging 256 scans. Data were analyzed using Omnic E.S.P v5.2 software. Nanogel morphology was imaged by cryo-transmission electronic microscopy (cryoTEM) on a JEOL JEM 2010 at 80 kV. TEM micrographs were analyzed using ImageJ (NIH, Bethesda, MD). At least 600 Ag NPs were analyzed per sample. The diameter distribution of Ag NPs was fitted to a Log-normal function. The amount of silver (wt%) in the NGs was determined by TGA using a Universal V4.1D TA Instruments (SDT Q600) with 2-4 mg samples under air atmosphere. The NG solutions were first dried and then dispersed in ethanol. This solution was placed in a platinum pan and heated to 80 °C at 10 °C/min. The sample was held at 80 °C for 2 h for complete removal of the ethanol and then allowed to cool down to room temperature. Next, the samples were heated to 100 °C at 10 °C/min and held for 30 min to ensure complete removal of moisture.

Then, the samples were heated to 675°C at 10 °C/min and held for 120 min to ensure complete removal of organic matter. Data were analyzed using TA Universal Analysis 2000 v4.5A.

Bacterial culture and antibacterial tests

S. aureus (ATCC®25923™) and *E. coli* (ATCC®25922™) were cultured in Trypticase Soy Broth (TSB) at 175 rpm and 37 °C for 12–16 h (overnight culture) and diluted to 10^8 CFU/ml using a 0.5X McFarland standard, a turbidity standard equivalent to 10^8 CFU/ml. To determine the minimum inhibitory concentration (MIC) as indicated by lack of visible bacterial growth, the standard broth dilution technique in Costar V-bottom 96-well (corning, Life Sciences) was employed. This test assesses the bacteria susceptibility to the hybrid NG, according to NCCLS M7-A4 (1997). The hybrid NG were serially diluted (1:1-1:512) with 100 μL of TSB inoculated with bacteria (10^6 CFU/mL), and incubated overnight, 37 °C. For each nanogel and bacterial strain, each 96 well plates contained negative (broth only) and positive growth (bacteria only) controls. On the same plates, NG1:1-Ag and NG1:4-Ag were tested in triplicate and NG1:8-Ag in duplicate. Results presented are the average of three independent 96-well plates per bacteria-type. In separate experiments, bacterial survival (10^5 CFU/mL) in the presence of the hybrid NGs (100 μg/mL) was assessed at 1 h, 5 h and 24 h by serial dilution and plating on 3M™ Petri films. Experiments were performed in triplicate.

Statistical analysis

The means and standard deviations (SDs) of the hydrodynamic diameter and diameter determined by cryo-TEM of the Ag nanoparticles, as well as the MIC and counts of viable bacteria are presented as average ± SD.

Results

The size distribution and hydrodynamic diameter (D_H) of the NG is given in Figure 1. At the concentrations in this study, all NGs display Gaussian size distributions. The D_H of the NG increases with lysozyme content. In particular, the average NG volume increases by around 3x for NG1:4 and 4x for NG1:8, relative to NG1:1.

The hydrodynamic diameter of the NG is maintained upon *in situ* reduction of Ag NPs (data shown in supplementary information) indicating that the incorporation of Ag does not significantly swell the NG. The neat NG, originally white in color, changes to dark/light brown because of the formation of Ag NPs (Figure 2). Note that the white color of the neat NG is due to the refractive index mismatch between the NGs and the solution which results in light scattering. The brown color of the NG loaded with NPs is due to the surface plasmon resonance (SPR) of Ag, following the *in situ* reaction that produces the NPs. Note that SPR is defined as the collective oscillation of electrons due to incident light. Figure 2 shows the UV-Vis spectra for the neat NG and hybrid NGs. The NG (Figure 2a) exhibits a shoulder at 280 nm characteristic of lysozyme, superimposed on the extinction scattering background that decays toward low values near 650 nm. In Figure 2b, the peak for the SPR of silver is noticeable only for NG1:1-Ag at 430 nm, which corresponds to the darkest solution. In contrast, NG1:4-Ag and NG1:8-Ag do not exhibit a SPR peak because of the larger

extinction scattering from the NG, as observed in the pictures of the NG solution (Figure 2). When cast on glass slides, NG1:4-Ag and NG1:8-Ag films are opaque whereas NG1:1-Ag is brown (Figure 3). To corroborate the presence of Ag NPs within the NG, the NG coated glass surfaces are exposed to UVO. UVO degrades the organic matter (i.e., dextran and lysozyme) leaving behind the exposed Ag NPs (i.e., brown). The kinetics of NG degradation is followed by UV-Vis and the corresponding spectra are shown in Figure 3. Note the characteristic behavior of each NG coating during degradation. For the NG1:1-Ag systems, the peak location and breadth for the SPR of Ag remains constant as the absorbance increases with NG degradation. Moreover, the peak for the SPR of Ag shows no shift in wavelength as compared to the solution, suggesting that the refractive index for NG1:1-Ag in solution and to the film are similar [16]. The SPR for NG1:4-Ag and NG1:8-Ag appears after 10 min UVO exposure at 432 nm and at 434 nm, respectively. The peak absorbance increases with UVO exposure for the former but remains nearly constant for the latter. Following 10 min exposure, NG1:8-Ag exhibits the greatest SPR breadth, which remains constant afterwards. In general, peak broadening and red shift are generally attributed to larger nanoparticles and/or the presence of aggregates.

Using cryo-TEM, the majority of the hybrid NG particles are round and isolated (Figure 4). The Ag NPs are located within the NGs and are not found in the space between NGs, consistent with successful removal of free Ag NPs by dialysis. At higher magnifications (inset), the sizes of the individual Ag NPs can be determined and are summarized in Table 1. Independent of the nanogel composition the embedded Ag NPs show Log-normal size distributions (Figure 4). For NG1:1-Ag the Ag NP diameter is 5.1 ± 0.2 nm. As the lysozyme concentration increases, the particle size decreases. For NG1:4-Ag and NG1:8-Ag, Ag NP diameters decrease to 2.8 ± 0.1 and 2.1 ± 0.2 nm, respectively. Because of limited statistics, the size of the hydrated hybrid NGs could not be accurately determined by cryo-TEM. Although cryo-TEM is an excellent technique to visualize colloidal systems in the hydrated state, cryo-TEM has a limited field of view which requires collecting many images to truly represent the entire sample [17].

The amount of silver (wt%) contained in the hybrid nanogels is measured by TGA (Table 1). Figure 5 shows the weight loss for pure dextran, pure lysozyme and the three hybrid NGs. Samples are held isothermally at 100 °C for 30 min to remove traces of water. With increasing temperature pure dextran exhibits an onset of thermal degradation at about 285 °C whereas pure lysozyme begins to degrade near 245 °C. When compared at T ~ 335 °C, dextran has lost about 70 wt% due to degradation of the glycoside ring, whereas lysozyme has lost only 30 wt%. Dextran has completely degraded by 525 °C, whereas lysozyme does not completely degrade until 650 °C has reached. The hybrid NG reflects the degradation characteristics of both dextran and lysozyme with the temperature stability of the hybrid NG increasing with lysozyme content. When compared at T ~ 335 °C, NG1:1-Ag, NG1:4-Ag and NG1:8-Ag have weight losses of 45 wt%, 38 wt% and 30 wt%, respectively. Note that NG1:8-Ag exhibits a similar weight loss profile as pure lysozyme at temperatures up to 550 °C. The residual weights relative to the dried sample (T = 100 °C) are summarized in Table 1. The residual silver is 5.7, 8.1 and 15.5 wt% for NG1:1-Ag, NG1:4-Ag and NG1:8-Ag, respectively. Prior to dialysis (data not shown), the residual weights relative to the dried samples are 12.9, 14.9 and 17.9 wt% for NG1:1-Ag, NG1:4-Ag and NG1:8-Ag,

respectively. These results indicate that the loading of Ag NPs and efficiency of the reaction (i.e., yield) inside the NG increases with lysozyme content and NG volume. In particular, after dialysis, NG1:1-Ag, NG1:4-Ag and NG1:8-Ag retain as much as 44, 54 and 87 wt% of the initial silver synthesized in the NG solution.

FTIR is used to characterize the NGs and hybrid NGs (Figure 6). The FTIR spectrum for NG1:1 is compared to pure lysozyme and dextran (Figure 6, top left) to facilitate the interpretation of the absorbance bands. The FTIR spectrum for pure lysozyme exhibits the characteristic amide I and amide II bands at 1655 and 1532 cm^{-1}, respectively. Other bands present in the lysozyme FTIR spectrum are 3300 cm^{-1} due to NH stretching, 1273 cm^{-1} due to CN stretching and NH bending, 1157 cm^{-1} due to CO stretching, 975 cm^{-1} due to CO, CC and COOH stretching and 833 cm^{-1} due to CH_2 rocking vibration [18, 19]. The FTIR spectrum of dextran exhibits a band at 2925 cm^{-1} due to stretching vibration of CH_2, a band at 1655 cm^{-1} characteristic of CO stretching, bands at 1485 and 1345 cm^{-1}, due to CH vibrational modes, and bands at 1011, 1111 and 1157 cm^{-1}, due to CO stretching vibration [20]. For the NGs containing Ag NPs, the intensities of some of the FTIR bands increase with Ag content. In particular, there is a broadening of the band at 1273 cm^{-1} (lysozyme only band) and the relative intensities of amide II (lysozyme only band) to amide I bands (dextran and lysozyme band) increase by ~ 5 fold with the presence of Ag NPs. This increase in absorbance is attributed to the SPR from the Ag NPs [21].

The results of tests of the antibacterial activity of the hybrid NG, assessed at different concentrations against *E. coli* and *S. aureus* are presented as MIC values appearing in Table 1. NG1:1-Ag shows the greatest antibacterial activity against *E. coli*, which exhibits a MIC that is about a third of the MIC for *S. aureus*. At concentrations up to 200 μg/mL, no antibacterial activity is measured for NG1:8 using the broth microdilution assay. NG1:4-Ag exhibits an intermediate antibacterial activity against *E. coli* and *S. aureus* with NG1:4-Ag marginally more effective against *E. coli*. Overall, *E. coli* is more sensitive than *S. aureus* to the antibacterial activity of the hybrid NG. For both *E. coli* and *S. aureus*, the MIC increases as the content of Ag NP and lysozyme increases, but decreases as the Ag NPs size increases.

To further evaluate antibacterial activity, the hybrid NGs were exposed to *E. coli* and *S. aureus* while agitating the medium. At this concentration, the hybrid NG particles contain 5.7, 8.1 and 15.5 μg of Ag per mL of NG1:1-Ag, NG1:4-Ag and NG1:8-Ag solution, respectively. All hybrid NGs inhibit *S. aureus* growth by ~2 logs at all times; this inhibition essentially keeps the NG-containing samples at their starting numbers, unlike the control which has proliferated during the experiment (Figure 7). In keeping with the greater sensitivity of *E. coli* to the NGs, no bacterial survival is measured after 5 h with NG1:4-Ag and NG1:8-Ag. NG1:1-Ag only reduces *E. coli* growth by 1 log within 1 h and 24 h.

Discussion

Current research in the area of Ag NPs focuses on exploiting their biological properties for applications such as disease diagnosis, treatment and therapeutics [4, 5]. Because of their versatility, the number of commercially available products containing Ag NPs is on the rise. For instance, Ag NPs can be found in textiles, water purification systems, paints and

biomedical devices [22]. Such widespread use of Ag NPs has endorsed concerns of its possible cytotoxicity. Although the mechanism by which Ag NPs induce cytotoxicity at high concentrations has not been clearly defined, cytotoxicity is believed to result from a combination of the release of Ag+ from the nanoparticles (main cause of toxicity) and particle ingestion [22]. Common cytotoxic effects with increased Ag NPs concentration include disruption of cell membrane, increased oxidative stress and impaired mitochondrial function, DNA binding and damage, and apoptotic cell death [23]. Therefore, we developed biocompatible dextran based NGs with embedded Ag NPs in solution to minimize their cytotoxicity. To create target delivery systems, these hybrid NG's can be functionalized by attaching ligands to the surface region. For example, preliminary studies show that IgG and R6.5 can be attached to NG1:1.

In previous work we developed hybrid NGs based on natural products without requiring additional chemicals other than a silver precursor. The synthesis of Ag NPs was carried out *in situ* in the NG solution. When using lysozyme and dextran NG prepared at a 1:1 stoichiometry, we obtained uniformly distributed Ag NPs within the NG. Furthermore, we demonstrated that loading of Ag in the NGs could be tuned by changing the concentration of silver precursor. In this paper, we focus on expanding the synthesis and stabilization of Ag NPs embed in the NG by varying lysozyme amount in the core of the NG, with antibacterial activity as an important readout. Although not apparent from UV-Vis spectra of hybrid NG in solution (i.e., no SPR) the increase in NG volume allows for greater loading of Ag NPs, as measured by TGA. In particular, the volume of the NG increases by 3x and 4x and the weight of Ag increases by 2x and 3x, for NG1:4-Ag and NG1:8-Ag relative to NG1:1-Ag, respectively. For all hybrid nanogels, the Ag NPs are uniformly dispersed in the NG (as detected by cryo-TEM). However, the size of the Ag NPs decreases as the lysozyme content increases, with sizes up to 2 nm in diameter for NG1:8-Ag. Particle size also can be estimated from the location of the Ag SPR. However, the comparison between different systems is not straightforward because the position, shape and intensity of the SPR depends on the dielectric constant of the particle and medium, the electronic interactions between the stabilizer and NPs, and the size, shape and the size dispersity [24]. For instance, Ag NPs (~ 5 nm) prepared *in situ* in dextran solution exhibit a SPR at 412 nm [7] whereas Ag NPs having similar size but prepared *in situ* in a NG1:1 solution exhibit a peak absorption at 430 nm. Furthermore, a blue shift of the SPR is expected as particle size decreases, whereas the results in Figure 3 showed a slight red shift. Namely, NG 1:4-Ag have 3nm Ag NPs which exhibit SPR at 432 nm whereas NG1:8-Ag contain 2 nm which exhibit a SPR at 434 nm. These discrepancies may be attributed to differences in the refractive indexes in the medium. Additionally; the breadth of the UVVis spectra reflects dispersion/aggregation of Ag NPs, which in our studies depend on the amount of lysozyme in the NG. Following UVO exposure of cast hybrid NGs (Figure 3), NG1:8-Ag shows the greatest Ag NP aggregation (e.g. widest breadth) suggesting higher stability of the Ag NPs within the NG as compared to NG1:1-Ag and NG1:4-Ag.

Previous findings show that biomolecules with carboxyl, hydroxyl and amine groups as well as polysaccharides (e.g., starch) can reduce and stabilize Ag NPs [25-27]. The use of lysozyme to synthesize Ag NPs in methanol was first reported using light activation [25],

which allowed for easy transfer into aqueous solution. In our study, the lysozyme is localized in the core of the nanogel, which is prepared and stored into aqueous solution. Because dextran is unable to reduce Ag ions, the formation of Ag NPs and their loading efficiency in hybrid NGs determined by the lysozyme content in the NG (as determined by TGA). Furthermore, the lysozyme contribution is confirmed by increased surface enhanced infrared absorption spectroscopy (SEIRAS) of the lysozyme characteristic bands (CN stretching and NH bending, 1280 cm^{-1}, and amide II, 1532 cm^{-1}) due to enhanced local electric field due to Ag NP near lysozyme. These results indicate that lysozyme promotes nucleation and stabilization of Ag NPs and limits their over growth within the NG.

The antibacterial activity of the hybrid NG is tested against *E. coli* ATCC®25922™, representative Gram negative bacteria, and *S. aureus* ATCC®25923™, representative Gram positive bacteria. *E. coli* represents a diverse group of bacteria that resides in the intestines. While most strains are harmless, some are pathogenic and can cause diarrhea or illness outside the intestinal track. The Gram-positive *S. aureus* is often carried on the skin or in the nose of healthy people and readily adheres to host proteins (e.g., fibrinogen, fibronectin) commonly adsorbed to biomaterials. This adherence can lead to formation of a biofilm that shelters and protects the pathogens against antimicrobial agents. This pathogen is among the most frequently reported pathogens that cause deep infection in hospitals. Our hybrid NGs are more potent towards Gram negative bacteria (Table 1, Figure 6), in keeping with other results in the literature [28-31]. The difference in the effects of silver on Gram negative versus Gram positive bacteria may lie in the structure of their cell wall. Gram negative bacteria are encased in a thin, negatively-charged, somewhat fragile outer lipopolysaccharide layer (7-8 nm) whereas Gram positive bacteria consists of a thick, highly-crosslinked rigid peptidoglycan layer (20-80 nm) that prevents Ag NPs from penetrating the layer. Other causes of greater susceptibility of Gram negative towards Ag NPs involve their effect on bacterial signal transduction (i.e., phosphorylation) which in turns affects cell growth.

Independent of bacterial type, the antibacterial activity of the hybrid NGs (measured as MIC) decreases as the amount of Ag NPs and lysozyme increases (e.g., Ag NP size decreases) in the NG solution up to NG1:8-Ag. This result is rather surprising considering that antibacterial properties of Ag NPs depend on size. Smaller Ag NPs exhibit better antibacterial properties because their larger surface area increases interaction and ionization compared to larger Ag NPs [2, 32]. Note, however, that NG1:1-Ag with 5 nm Ag NPs exhibits a lower MIC (2.1 μg/mL) than that of 5 nm bare Ag NPs (MIC~5 μg/mL) [33]. Interestingly, using the standard method of determining MIC, i.e., broth microdilution assays, no clear breakpoint could be found for NG1:8-Ag, although significant antibacterial effects are observed with NG1:8-Ag in our time course studies. That is because the antibacterial properties of Ag NPs also depend on their stability in solution [34]. In our system, Ag NPs are embedded within the NG and results point to better stabilization of Ag NPs in NG1:8-Ag. Furthermore, upon UVO exposure the Ag NPs in NG1:8-Ag aggregate faster (by UV-Vis, Figure 4) as compared to NG1:1-Ag and NG1:4-Ag (Figure 3) and do not inhibit growth at static conditions (Table 1). The Ag NP stabilization is overcome by shaking the solution, promoting diffusion of smaller particles and thus, increased killing

(Figure 7). In particular, the hybrid NGs exhibit increased bactericidal properties with increasing Ag content towards *E. coli*. Like the other hybrid NGs, it exhibited only bacteriostatic properties towards *S. aureus*. The differences in activity allow for tuning the hybrid NGs for specific applications. For instance, to prevent biofilm formation, a more diffusive bactericidal agent loaded into the NGs may be the most effective means of infection prevention. Thus, the tunability of the different hybrid NGs makes it possible to optimize Ag release for specific clinical use, type of infection, allowing appropriately targeted drug delivery to minimize complications that may occur with use of antimicrobial agents.

Conclusions

We have prepared dextran based hybrid nanogels with varying lysozyme content, studied its role in the size and loading of AgNPs and evaluated how that, in turn, affects their antibacterial activity. An increase in lysozyme content results in larger nanogels with smaller Ag NPs, greater loading but higher MIC. This trend is reversed by promoting diffusion of Ag out of the nanogel, suggesting lysozyme plays a key role in the stabilization of Ag NPs. To sum up, this work introduces a hybrid nanogel that can be optimized to release Ag as needed for specific biological applications.

Supplementary Material

Refer to Web version on PubMed Central for supplementary material.

Acknowledgments

Prof. Cherie Kagan for FTIR, Dr. Dewight R. Williams for TEM imaging, and NSF CERMRI for facility use. Ms. Dastgheyb's work was supported by the NIH (National Institute of Arthritis and Musculoskeletal and Skin Diseases) training grant T32-AR-052273. The National Institutes of Health provided support via grants R01HL060230 (D.M.E), R01-EB006818 (D.M.E., R.J.C.), HD061053 and DE019901 (N.J.H.). A pilot grant from NSF Nano-Bio Interface Center DMR08-32802 (R.J.C., D.M.E. and N.J.H.) facilitated this work, as well as partial support from NSF DMR09-07493 (RJC). Facilities at the Nanoscale Characterization Center supported by NSF/CEMRI (DMR11-20901) are acknowledged.

References

1. Conde J, Doria G, Baptista P. Noble metal nanoparticles applications in cancer. J Drug Delivery. 2012; 2012:12.
2. Morones JR, et al. The bactericidal effect of silver nanoparticles. Nanotechnology. 2005; 16(10): 2346–2353. [PubMed: 20818017]
3. Rai M, Yadav A, Gade A. Silver nanoparticles as a new generation of antimicrobials. Biotechnol Adv. 2009; 27(1):76–83. [PubMed: 18854209]
4. Nair LS, Laurencin CT. Silver nanoparticles: Synthesis and therapeutic applications. J Biomed Nanotech. 2007; 3(4):301–316.
5. Bhattacharya R, Mukherjee P. Biological properties of "naked" metal nanoparticles. Adv Drug Deliv Rev. 2008; 60(11):1289–1306. [PubMed: 18501989]
6. Ferrer MCC, Eckmann UN, Eckmann DM, Composto RJ. Hemocompatibility and biocompatibility of antibacterial biomimetic hybrid films. Toxicol Appl Pharmacol. 2013; 272(3):703–712. [PubMed: 23933530]
7. Ferrer MCC, Hickok NJ, Eckmann DM, Composto RJ. Antibacterial biomimetic hybrid films. Soft Matter. 2012; 8(8):2423–2431. [PubMed: 23807896]

8. Lu RQ, Yang DP, Cui DX, Wang ZY, Guo L. Egg white-mediated green synthesis of silver nanoparticles with excellent biocompatibility and enhanced radiation. Int J Nanomedicine. 2012; 7(1):2101–2107. [PubMed: 22619546]
9. Shanmukh S, Jones L, Zhao YP, Driskell JD, Tripp RA, Dluhy RA. Identification and classification of respiratory syncytial virus (RSV) strains by surface-enhanced Raman spectroscopy and multivariate statistical techniques. Anal Bioanal Chem. 2008; 390(6):1551–1555. [PubMed: 18236030]
10. Tse C, Zohdy MJ, Ye JY, O'Donnell M, Lesniak W, Balogh L. Enhanced optical breakdown in KB cells labeled with folate-targeted silver-dendrimer composite nanodevices. Nanotechnol Bio Med. 2011; 7(1):97–106.
11. Ferrer MCC, Ferrier RCJ, Eckmann DM, Composto RJ. A facile route to synthesize nanogels doped with silver nanoparticles. J Nanopart Res. 2013; 15(1)
12. Li J, Yu SY, Yao P, Jiang M. Lysozyme-dextran core-shell nanogels prepared via a green process. Langmuir. 2008; 24(7):3486–3492. [PubMed: 18302424]
13. James C, Johnson AL, Jenkins ATA. Antimicrobial surface grafted thermally responsive PNIPAM-co-ALA nano-gels. Chem Commun. 2011; 47(48):12777–12779.
14. Wu W, Zhou T, Berliner A, Banerjee P, Zhou S. Smart core-shell hybrid nanogels with Ag nanoparticle core for cancer cell Imaging and gel shell for pH-regulated drug delivery. Chem Mater. 2010; 22(6):1966–1976.
15. Clarke, HT. Handbook of organic analysis. Lowe and Brydone Printers Ltd; London: 1949.
16. Willets KA, Van Duyne RP. Localized surface plasmon resonance spectroscopy and sensing. Ann Rev Phys Chem. 2007; 58:267–297. [PubMed: 17067281]
17. Mittal, V.; Matsko, NB. Engineering Materials. Springer-Verlag; Berlin Heidelberg: 2012. Analytical imaging techniques for soft matter.
18. Barth A. The infrared absorption of amino acid side chains. Progr Biophys Mol Bio. 2000; 74(3-5): 141–173.
19. Kong J, Yu S. Fourier transform infrared spectroscopic analysis of protein secondary structures. Acta Biochim Biophys Sin. 2007; 39(8):549–559. [PubMed: 17687489]
20. Heyn ANJ. The infrared absorption of dextan and its bound water. Biopolymers. 1974; 13:475–506. [PubMed: 4833336]
21. Caro, C.; Castillo, PM.; Klippstein, R.; Pozo, D.; Zaderenko, AP. Silver Nanoparticles: sensing and imaging applications. 2010. www.chemopen.com
22. Reidy B, Haase A, Luch A, Dawson KA, Lynch I. Mechanisms of silver nanoparticle release, transformation and toxicity: A critical review of current knowledge and recommendations for future studies and applications. Materials. 2013; 6(6):2295–2350.
23. Suresh AK, Pelletier DA, Wang W, Morrell-Falvey JL, Gu B, Doktycz MJ. Cytotoxicity induced by engineered silver nanocrystallites is dependent on surface coatings and cell types. Langmuir. 2012; 28(5):2727–2735. [PubMed: 22216981]
24. Moores A, Goettmann F. The plasmon band in noble metal nanoparticles: an introduction to theory and applications. New J Chem. 2006; 30(8):1121–1132.
25. Eby DM, Luckarift HR, Johnson GR. Hybrid antimicrobial enzyme and silver nanoparticle coatings for medical instruments. Acs App Mater Interfaces. 2009; 1(7):1553–1560.
26. Sun XP, Luo YL. Preparation and size control of silver nanoparticles by a thermal method. Mater Lett. 2005; 59(29-30):3847–3850.
27. Vigneshwaran N, Nachane RP, Balasubramanya RH, Varadarajan PV. A novel one-pot 'green' synthesis of stable silver nanoparticles using soluble starch. Carbohyd Res. 2006; 341(12):2012–2018.
28. Alarcon EI, et al. The biocompatibility and antibacterial properties of collagen-stabilized, photochemically prepared silver nanoparticles. Biomaterials. 2012; 33(19):4947–4956. [PubMed: 22494887]
29. dos Santos CA, Jozala AF, Pessoa A, Seckler MM. Antimicrobial effectiveness of silver nanoparticles co-stabilized by the bioactive copolymer pluronic F68. J Nanobiotechnology. 2012; 10

30. Radzig MA, Nadtochenko VA, Koksharova OA, Kiwi J, Lipasova VA, Khmel IA. Antibacterial effects of silver nanoparticles on gram-negative bacteria: Influence on the growth and biofilms formation, mechanisms of action. Colloids Surf B. 2013; 102:300–306.

31. Taglietti A, et al. Antibacterial activity of glutathione-coated silver nanoparticles against gram positive and gram negative bacteria. Langmuir. 2012; 28(21):8140–8148. [PubMed: 22546237]

32. Panacek A, et al. Silver colloid nanoparticles: Synthesis, characterization, and their antibacterial activity. J Phys Chem B. 2006; 110(33):16248–16253. [PubMed: 16913750]

33. Li W-R, Xie X-B, Shi Q-S, Zeng H-Y, Ou-Yang Y-S, Chen Y-B. Antibacterial activity and mechanism of silver nanoparticles on Escherichia coli. Appl Microbiol Biotechnol. 2010; 85(4): 1115–1122. [PubMed: 19669753]

34. Kvitek L, et al. Effect of surfactants and polymers on stability and antibacterial activity of silver nanoparticles (NPs). J Phys Chem C. 2008; 112(15):5825–5834.

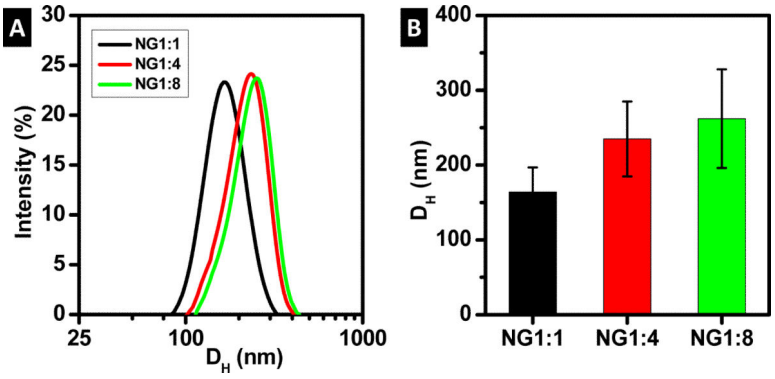

Figure 1.

NG diameters measured by DLS: a) intensity distribution of NG diameter and b) hydrodynamic diameter (D_H)

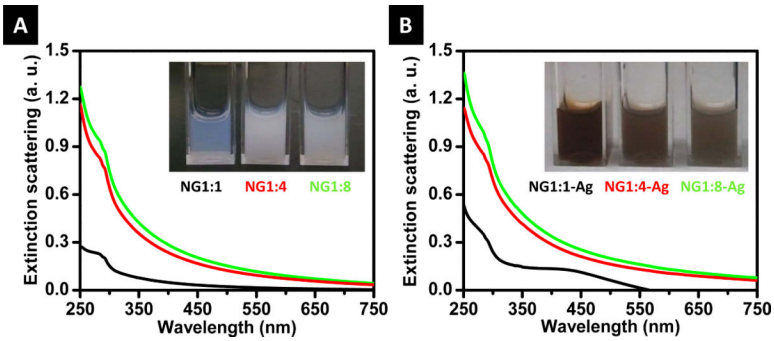

Figure 2.

UV-Vis spectra for NG in aqueous solution: a) prior and b) subsequent to *in situ* synthesis of Ag NPs. Insets are photographs of NG solutions.

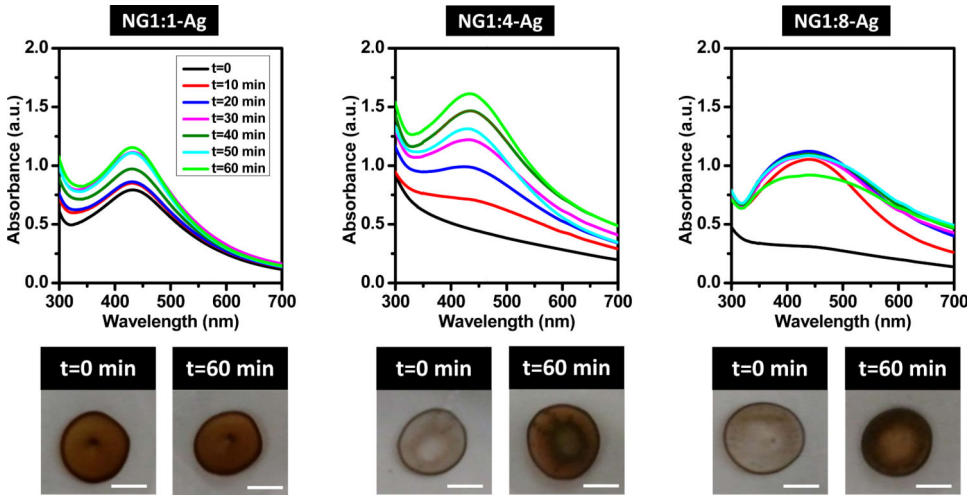

Figure 3.

Kinetics of NG degradation upon exposing hybrid NGs cast on glass slides to UVO for 0 to 60 min. Top images are UV-Vis spectra for as-prepared (t = 0 min) and UVO exposed hybrid NGs. The bottom photographs show images for t = 0 min and t = 60 min (scale bar, 500 mm). Note the color changed from white (t = 0 min) to brown (t = 60 min) for the both NG1:4-Ag and NG1:8-Ag systems.

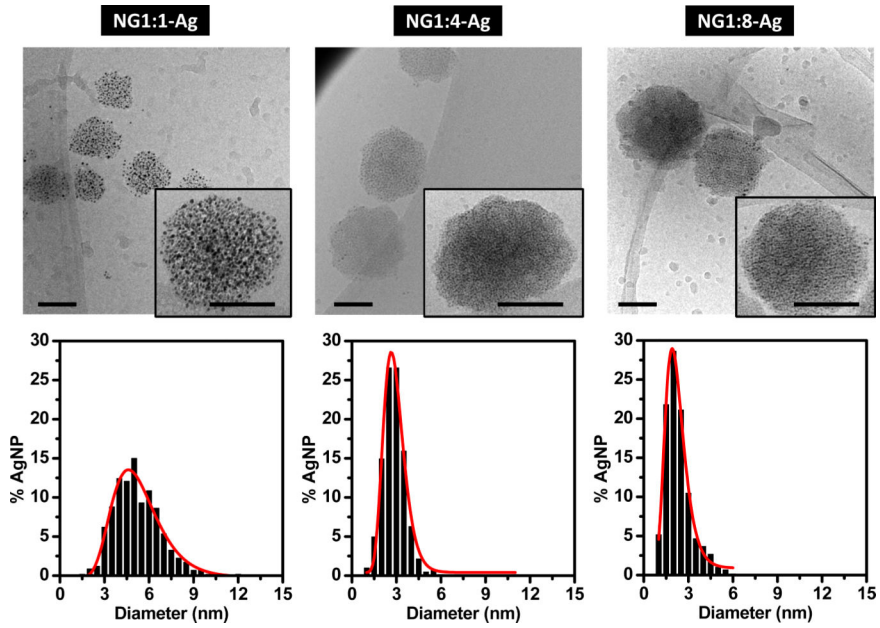

Figure 4.

Top images are cryo-TEM micrographs of the hybrid NG (scale bar, 100 nm). Bottom plots are histograms of Ag NP diameters. The red lines are log-normal fits. The average diameters of Ag NPs in NG1:1-Ag, NG1:4-Ag and NG1:8-Ag are 5.1 ± 0.2, 2.8 ± 0.1 and 2.1 ± 0.2 nm, respectively.

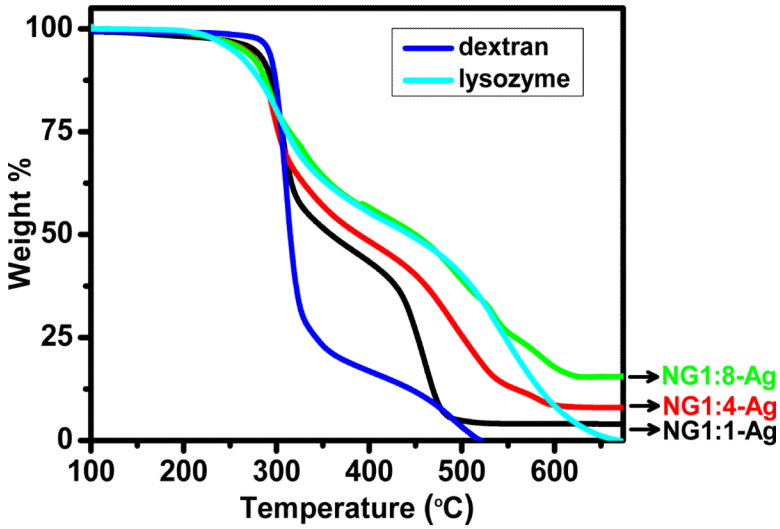

Figure 5.

TGA weight loss curves for dextran, lysozyme and hybrid NGs in air. All samples were dried at 100 °C prior to heating.

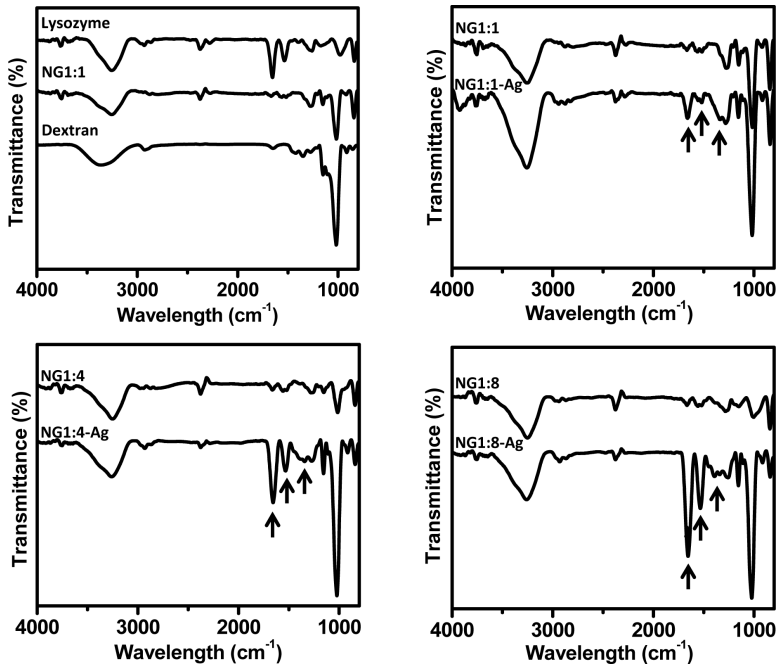

Figure 6.

FT-IR spectra for lysozyme, dextran, NG and hybrid NG. Arrows denote characteristic lysozyme amide I, amide II, and CN stretching and NH bending bands at 1655, 1532 and 1280 cm^{-1}, respectively.

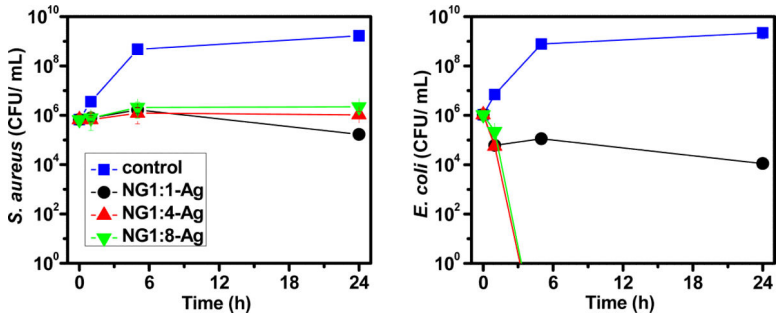

Figure 7.

Viable bacteria, expressed as colony-forming units per mL (CFU/mL), following incubation with hybrid NGs over time. As a control, a bacteria solution without hybrid NGs was used. Results shown are the average of three independent experiments (± S.D.) for a representative experiment in three independent repeats. Unseen error bars are small and obscured by the symbol.

Table 1

Summary of diameter distributions of Ag NPs in NG determined by cryo-TEM, the weight percent of Ag within the NG as measured by TGA and minimum inhibitory concentration (MIC) of hybrid NGs. D_C is the center of the Log-normal fit.

Sample	Ag diameter (nm) cryo-TEM		Ag wt.% TGA	MIC (μg/mL)			
				S. aureus		*E. coli*	
	D_C (nm)	As prep	After dialysis	NG	Ag	NG	Ag
NG1:1-Ag	5.1 ± 0.2	12.9	5.7	100	5.7	36 ± 13	2.1 ± 1
NG1:4-Ag	2.8 ± 0.1	14.9	8.1	100	8.1	78 ± 26	6.2 ± 2
NG1:8-Ag	2.1 ± 0.2	17.9	15.5	— *a)*		— *a)*	

*a*No antibacterial activity was detected using the broth microdilution assay.